A CCD Spectropolarimeter for the Lick Observatory 3-Meter Telescope

J.S. MILLER, L.B. ROBINSON, AND R.W. GOODRICH

Abstract

An improved spectropolarimeter and imaging polarimeter for the wavelength range 4000 Å to 7600 Å is described, along with data analysis procedures and error analysis. The spectropolarimeter has approximately 20 times higher efficiency than the Pockels cell IDS system used previously.

1. Introduction

For some years we made considerable use of a very successful spectropolarimeter incorporated into the Lick 3-m Cassegrain spectrograph. This instrument, described in detail by Miller, Robinson and Schmidt [1], (hereinafter MRS), used the image-tube, image-dissector system (IDS) as the detector and a Pockels cell modulator. The Pockels cell operated as a switchable quarter-wave retarder, with modulation frequencies typically in the range 0.2 to 0.5 Hz. When we modified the spectrograph to allow CCDs to be used as detectors, a large (> 7) increase in spectrograph speed was achieved. It was clear that the spectropolarimeter should also be modified, to take advantage of the higher throughput. However, because of the relatively long read-out time of the CCD, it was obvious that the system would have to be changed considerably to permit the use of the CCD.

This paper describes the modifications to the spectrograph for CCD use, several alternative approaches to spectropolarimetry we tried, and the final system we developed, which is now in regular use.

2. CCD Cassegrain Spectrograph

The CCD version of the Cassegrain spectrograph is a straightforward modification of the one described by MRS. There are two configurations available: one using refractive optics and grisms (the "lens/grism spectrograph") and the second using a Schmidt camera (the "UV Schmidt spectrograph"). Both use the original TV guiding system (though that has now been upgraded with a CCD TV system; (ROBINSON [2]), slit assembly, and filter wheels. The lens/grism system is a "straight-through" design. Below the slit the light encounters the filter wheels (a total of three), a collimating lens consisting of an 82.5 mm diameter, 711 mm focal length cemented achromat which provides a 41.3 mm beam, a grism, a Nikon

Noct-Nikkor 58 mm f/1.2 camera lens, the dewar window, and the CCD detector. In the UV Schmidt mode, the refracting optics are all removed, and, the system is identical to that described in MRS. A new Schmidt camera was constructed, identical in layout to the original one except for a bigger back focal distance needed to reach the CCD in its dewar.

Both configurations are fully remote controllable, though interchanging between them is a manual task which takes about 30 minutes; generally an observer uses one or the other for the entire night. The lens/grism system operates between 4000 and 8500 Å, the limits being set by the transmission of the lenses. It provides dispersions of about 2.8 to 10 Å/pixel with a Texas Instruments 800 × 800 three phase CCD (15 micron pixels). Up to three grisms can be installed at one time, and a fourth position of the grism tray removes all grisms from the beam for direct work. There is also a transmission echelle grism that can be cross dispersed with a grism, providing about 1 Å/pixel resolution. The throughput of the echelle system is relatively low, so it is not used heavily. The quantum efficiency of the lens/grism system including the telescope optics and the detector reaches a peak of about 25% when a 420 g/mm grism giving about 5 Å/pixel is used. The peak quantum efficiency of the UV Schmidt is about half of this because of greater light losses in the Schmidt camera. However the Schmidt system works over the entire range from 3000 to 11000 Å. In the ultraviolet ($\sim$ 3500 Å) the total quantum efficiency of the telescope plus spectrograph plus detector is about 6%. The UV Schmidt system can make use of any of three installed gratings, though one grating can be replaced by a flat mirror for direct imaging. The direct field is about 2 arcminutes in diameter.

The same detector can be mounted in either configuration. For the lens/grism mode, the dewar attaches to an X-Y stage. One direction of motion is along the dispersion, allowing one to choose a central wavelength, while the perpendicular motion allows positioning of the CCD so as to minimize the impact of CCD flaws. The details of the CCD electronics, CCD UV enhancements, and data-taking system are described elsewhere (ROBINSON et al. [3]).

While the performance of the spectrograph described here is excellent, there are some obvious places where improvement is possible. The Nikon lens has some residual chromatic aberration, which means that some refocussing is needed as the central wavelength is changed; the focus problem becomes much worse in the near infrared. The UV Schmidt system suffers from excessive light losses in the Schmidt camera, largely from the need to have an overly large hole in the folding flat. This need stems from the requirement that the camera focal position be a fair distance behind the surface of the folding flat to match with the CCD position in its dewar. Were it possible to dedicate a CCD to this system, better perfomance could be achieved. Nevertheless, because of the superb UV response of the detector, the UV Schmidt configuration is one of the most efficient in the UV available anywhere. We plan the following major improvements: changing the device into a double beam spectrograph with a dichroic splitter and replacing the existing cameras with two all-refracting custom lenses similar to those discussed during this Workshop by Epps. We expect the performance improvement to be considerable.

3. Spectropolarimeter

We tried several approaches to converting the spectropolarimeter described in MRS to one using a CCD. While we rejected all but one, it is worthwhile to examine the rejected ones for the lessons they provide.

3.1 Charge Shifting

The first approach was to use the Pockels cell system exactly as before, but use the CCD itself as an intermediate storage device during modulation. It was realized several years ago that the ability to move a recorded image within the CCD could be used for special instrumental applications. The "drift scan" technique, with the image from the telescope drifting across the CCD in exact synchronism with the clocking of the recorded image within the CCD, was used by Mackay [4] to help remove effects due to non-uniform CCD response from recorded CCD images. A similar technique is planned by workers at Steward Observatory [5] to continuously record a long strip of the sky as it passes over a motionless telescope.

It was also suggested by the Steward group that the ability to move charge on the CCD could help in the image chopping needed for polarimetry. Since the three phase CCD allows images to be shifted either "up" or "down" by merely changing clock phase, one could expose one polarization state for a second, then shift the image and expose the other polarization state on the same part of the CCD, then shift the image back and repeat the process until enough signal was built up. Part of the CCD would be masked for temporary storage of each image while inactive. The result would be two images on the CCD, taken with different polarization states, but recorded on the exact same pixels of the CCD, so that non-uniform response of the CCD would cancel.

Software was developed for the Lick CCD controller and for the data acquisition computer to test this on-chip image chopping scheme. An image could be shifted by 200 rows or more in a few milliseconds at intervals from 200 milliseconds to several seconds. Exposing with this mode should result in identical dual images.

The test was intended to check that a stellar image or spectrum on faint sky background could be shifted many times back and forth without losing or smearing part of the data. We found two unexpected problems!

On several different CCDs, when exposed while image chopping for a few minutes, at light levels corresponding to about one electron per pixel per second, we found many very bright pixels with dark columns many rows long, either above or below the bright pixel. The bright pixels were distributed in various random patterns, different on different CCDs, but constant on any one CCD. Janesick at JPL [6] was easily able to duplicate this result, and dubbed it the "Lick effect." He also suggested an explanation [7, 8]:

Suppose that the potential wells on the CCD have occasional irregularities that interfere with charge transfer in one direction or the other. These "charge pockets" may have capacities of less than 50 electrons, and would be unnoticed at normal exposure levels. In this circumstance, if for example we shift 200 rows every 400 msec and have a signal level of 1 electron per second per pixel, then a

20 electron pocket would collect all the charge in 50 rows. When shifting back, the excess 20 electrons would stay together in a single pixel, which on the next forward shift would be added to the contents of the pocket on the final step. Even a very small pocket such as this one would end up with 1000 electrons after 50 transfers forward and back, and the pixels whose charge had been stolen would be dark.

Running the image chopping program with no input light demonstrated a second problem. The apparent dark signal increased dramatically when image chopping was done. This apparently clock-generated signal should have been no surprise, since it is well known that the serial clocks must be stopped during long exposures to prevent excess signal on the rows near the serial register. The parallel clocks can also generate excess charge.

The "Lick effect" has been seen at some level on every CCD tested, including a thinned TI 500 × 500, several thinned TI 800 × 800 and a GEC 385 × 576 front-illuminated CCD. This turns out to be an excellent diagnostic tool [7], pinpointing pixels that have charge transfer problems for low signal level. The regions on the CCDs that show the effect most strongly have proven also to be least satisfactory for normal low light level spectroscopy. We have been unable to eliminate the pockets by adjusting clock amplitudes, although some CCDs are better than others.

The excess dark current from image chopping is device-dependent and could probably be reduced by tailoring the parallel clock waveforms. However, the combination of charge pockets and excess dark current due to image shifting make it clear that the image shifting method is undesirable for very high precision work, and alternative techniques for polarimetry measurements were considered.

3.2 Slow Modulation of Pockels Cell

We next considered modes which took advantage of the superb photometric stability of the CCD. Flat fields taken days or even weeks apart, if done carefully, are repeatable to a fraction of a percent. This suggested that, since the polarimeter is a double-beam device with light of perpendicular polarization states being recorded simultaneously, the modulation frequency could be made so low that the chip could be read out each time before a modulation. Since the readout time is roughly a minute, this means exposure times of at least several minutes per state of the device were needed for reasonably efficient observing. In fact this approach worked very well. We exposed for several minutes with the Pockels cell held at constant potential, read out the CCD, reversed the potential on the cell, took a second exposure, and read it out. Since all light was being recorded in both exposures, appropriate combination of the data allowed us to extract one of the Stokes parameters as a function of wavelength (the procedure to do this is described below, as it is the same for the device we finally adopted). Rotation of the instrument by 45° followed by a second set of observations allowed the second Stokes parameter to be determined. While this gave results as reliable as the old system in spite of the slow modulation, we found that the Pockels cell could not stand up to DC operation; it gradually became cloudy. We subsequently learned, contrary to earlier information on the matter, that this was probably inevitable for any Pockels cell in DC operation, even those with grid wires rather than a conductive coating for supplying the potential.

We abandoned this approach.

3.3 Calcite Crystal

Once the idea of very slow modulation is accepted, made possible by the extremely high stability of the CCD detector and a two-beam polarimeter, other possibilities can be explored. For example, we tried the very simple approach of using a piece of calcite 41 mm long located just below the slit. This produced two in-line, perpendicularly polarized images of a 15 arcsec portion of the slit, so that two spectra were recorded simultaneously. Modulation was produced by rotating the entire spectrograph through four positions spaced 45° apart, a complete exposure being taken at each setting. While this worked fairly well, the small amount of flexure in the spectrograph caused the CCD fringe pattern to shift slightly on the chip from exposure to exposure, making flat-fielding problematical at the level required for this approach to work. Also the rotation of the slit on the sky opened up the possibility of different sampling of extended objects at different position angles. While we felt that over all a "calcite-only" spectropolarimeter was certainly feasible, we abandoned it for what we feel is a much more satisfactory design.

3.4 Rotatable Waveplate

3.4.1 The instrument

The undesirability of rotating the entire spectrograph to four position angles to measure linear polarization led us to consider rotating instead the plane of incoming light by means of a half-wave retarder. We had Meadowlark Optics of Longmont, Colorado fabricate a so-called "superachromatic" half-wave retarder with a diameter of 50 mm. The broad band character of the device is achieved by using multiple sheets of a polymer plastic cemented between two quartz cover glasses. The fast axes of the sheets are rotated with respect to one another. The result is a waveplate that produces a retardation within a few percent of a half wave from 3200 to 7200 Å. We mounted the retarder in the same place that the Pockels cell used to occupy, about 42 cm above the spectrograph slit. It is mounted in a rotatable stage whose position angle can be set by remote control to an accuracy of less than 0°.5.

Because the previously-used calcite crystal would only allow a 15 arcsecond slit and significantly bigger crystals were extremely expensive, we chose a different approach to beam separation. We had the Karl Lambrecht Co. specially construct for us a cemented pair of their broad-band polarizing beam-splitting cubes. Two of these operating together effectively produce two perpendicularly polarized beams traveling parallel to one other with very little light loss; the polarimetric purity of each beam is very high (extinction greater than 100:1). The beamsplitter works from 4000 to 7000 Å, and the 12 mm cube face allows a 30 arcsecond slit length. The cubes are located in the filter wheel directly beneath the slit.

For the measurement of a Stokes parameter of linear polarization, an exposure is taken with an initial position of the retarder, the CCD is read out, the retarder is rotated 45°, and a second exposure of the same length is taken and read out.

The other Stokes parameter is derived from two exposures taken with the retarder rotated 22°.5 and 67°.5 from its initial position. The spectrograph remains fixed for all observations.

With the grism removed (or other grating replaced with a flat) the spectropolarimeter becomes an imaging polarimeter. The field of view, set by the beam-splitting cubes, is 30 arcseconds on a side. The sequence of observations is identical.

3.4.2 Data reduction

The reduction of a complete observation set to the set of Stokes parameters is done within the image-processing system *VISTA* (LAUER et al. [9]). We have used the spectropolarimeter only to measure the linear polarization and total intensity and this somewhat simplifies the reduction. If both linear and circular polarization were measured the technique described below would have to be modified slightly to account for the slight mixing of circular polarization into the linear polarization and vice versa.

Several assumptions are made in the data reduction, the most fundamental being that the characteristics of the instrument are constant with time. With the IDS spectropolarimeter this was not a good assumption. For example, during a long exposure the position of the sweeps across the cathode face might drift, yielding a time-variable detection efficiency and destroying the reliability of the polarization measurements. However the stability of the CCD detector has been amply demonstrated in tests such as the measurement of zero-polarization stars ("null standards"). The further assumption of negligible instrumental polarization is based on actual measurements. Using either the Pockels cell or the waveplate version of the spectropolarimeter and rotating the "tub" (hence the entire spectrograph) we can obtain redundant sets of Stokes parameters for a given star which differ only by the polarization introduced by the spectrograph itself. Such measurements of the null standards BD+35° 3956, HD 165908, and HD 109055 indicate instrumental Stokes parameters of $Q(instr) = +0.003 \pm 0.036$ % and $U(instr) = -0.003 \pm 0.057$ %. These values are much smaller than our typical observational uncertainties and therefore in general we ignore the instrumental polarization. (In any case the software allows for removal of the instrumental Stokes parameters if necessary.)

Two other assumptions involve the characteristics of the waveplate. To be able to smooth the position angle (p.a.) correction curve as a function of wavelength we assume that the fast axis of the waveplate is a slowly-varying function of wavelength. The unsmoothed p.a. correction curves give ample justification for this assumption. We also must assume that very little circular polarization is mixed into our linear polarization measurements. This is true if either the circular polarization, V, is small or if the waveplate's retardance is accurately half-wave at all wavelengths. In most astrophysical circumstances the optical circular polarization may indeed be neglected, but even in cases where it is significant the achromatic waveplate which we are using is within 0.02λ of halfwave from 4000 to 7000 Å so that the assumption of negligible mixing is a good one. (Evidence for the latter is also that the "polarizance," or the value measured for 100% linearly polarized light, is essentially indistinguishable from 100% across most of our operational wavelength range.)

3.4.3 The method

Two sets (of two spectra each) are used to determine a given linear Stokes parameter. We will call these sets A and B, and because the spectra appear as two vertical strips on the TV screen of the data-taking system on Mount Hamilton, we will use the subscripts L and R to refer to the left and right spectra (respectively) of a given set. (Thus the four spectra are designated A_L, A_R, B_L, and B_R.) The total spectral intensity of light coming through the spectrograph slit is I_A for set A and I_B for set B. Because of guiding errors and transparency changes, these two are not identical.

It is useful in some respects to consider separately the spectrograph above and below the beamsplitter. The first part we will represent by the fraction of light in the two orthogonal senses of polarization, designated p_0 and p_{90} so that $p_0 + p_{90} = 1$ and $p_0 = p_{90} = 0.5$ for unpolarized light. After the beamsplitter these two are separated and it is useful to consider the beams separately. The spectrograph throughput of each beam will be represented by f_0 and f_{90}, while the detector quantum efficiency may be represented by $\eta_{0,ij}$ and $\eta_{90,ij}$, where the ij explicitly recognizes the fact that the detector efficiency is a function of the pixel upon which the light falls. Using this notation we may write the recorded values of the four spectra:

$$\begin{aligned} A_L &= I_A\, p_0\, f_0\, \eta_{0,ij} \quad ; \quad A_R = I_A\, p_{90}\, f_{90}\, \eta_{90,ij} \\ B_L &= I_B\, p_{90}\, f_0\, \eta_{0,ij} \quad ; \quad B_R = I_B\, p_0\, f_{90}\, \eta_{90,ij}. \end{aligned} \tag{1}$$

The first correction applied to the data is to divide by a flat field exposure. This removes the pixel-to-pixel sensitivity variations η_{ij} and the beam throughputs f, but because flat fields are usually taken using partially polarized light (light reflected from the inside of the dome, twilight sky, etc.) there will be introduced another factor representing the polarization of the source, p'. This factor enters into the calculations in a manner analogous to the throughputs f (it is as if the throughputs changed when the flat field was taken), and because the normalized Stokes parameter is given by a ratio of the form

$$Q = \frac{A_L - B_L}{A_L + B_L}, \tag{2}$$

these factors cancel out and do not affect the final result. However the intensities I_A and I_B do not cancel out of the above equation, and hence the ratio $\omega = I_A/I_B$ needs to be calculated and this correction applied. To calculate ω we first convert each two-dimensional image into a pair of sky-subtracted spectra. Then ω is given by

$$\omega = \frac{I_A}{I_B} = \sqrt{\frac{A_L\, A_R}{B_L\, B_R}}\,. \tag{3}$$

In general we expect ω to be a slowly-varying function of wavelength so we usually smooth the resulting $\omega(\lambda)$ before multiplying B_R and B_L by it. The Stokes parameter may now be calculated in two ways:

$$Q_L = \frac{A_L - \omega B_L}{A_L + \omega B_L} \quad ; \quad Q_R = \frac{\omega B_R - A_R}{\omega B_R + A_R}. \tag{4}$$

If ω has not been smoothed then $Q_L = Q_R$; if ω has been smoothed then the average $(Q_L + Q_R)/2$ is formed and has somewhat smaller pixel-to-pixel noise. (It should be noted that a set of observations taken through a Polaroid filter is reduced in a similar fashion to create the polarizance and position angle correction curves.)

At this stage $Q(\lambda)$ and $U(\lambda)$ are in the "observed frame," which rotates as a function of wavelength due to the rotation of the fast axis of the waveplate with wavelength. The position angle correction curve is applied to the Q and U spectra to form $Q(\lambda)$ and $U(\lambda)$ in the usual "sky reference frame." The zero-point of this calibration is determined from observations of polarized stars with published, well-determined position angles.

3.4.4 Calibration and tests

As already mentioned we observe the dome through a Polaroid filter with our instrument to calculate the polarizance and p.a. correction curves. The zero point of the latter curve is dependent upon two instrumental parameters — the "zero point" or nominal position of the waveplate's fast axis and the rotation of the beamsplitter within its holder. Both of these are stable to $\lesssim 0\overset{\circ}{.}3$. The zero point of the correction curve is observationally determined by measuring the position angles of polarization standard stars and comparing our measurements with the published values. In Fig. 1(b) we present a composite p.a. correction curve from 3320 to 8100 Å.

In Fig. 1(a) we show the measured polarizance of the system. This is the efficiency at which the polarimeter can measure light which is 100% polarized. As can be seen from the figure the polarizance is essentially unity from 4000 to 7600 Å.

A test of the reduction technique was performed on a null standard star. To simulate the effects of a poorly guided sequence of observations, we took one exposure normally, followed by a second one in which the star was purposely removed from the slit halfway through the exposure. In a single-beam instrument the second observation in the latter set would have only half of the number of counts as the first observation in that set, and hence the single-beam polarimeter would measure 33% polarization — clearly a major error! However the two-beam instrument and its data reduction procedures accurately reduce this observation set to zero polarization. Figure 2 shows one example of this type of test, in which the final mean value of Q is $-0.031 \pm 0.015\%$. (The measured value of Q for the well-guided observation set was $-0.033 \pm 0.013\%$.)

Finally in this section we present Fig. 3, a plot of the expected uncertainty in a Stokes parameter (here taken as Q) versus the V magnitude of the object.

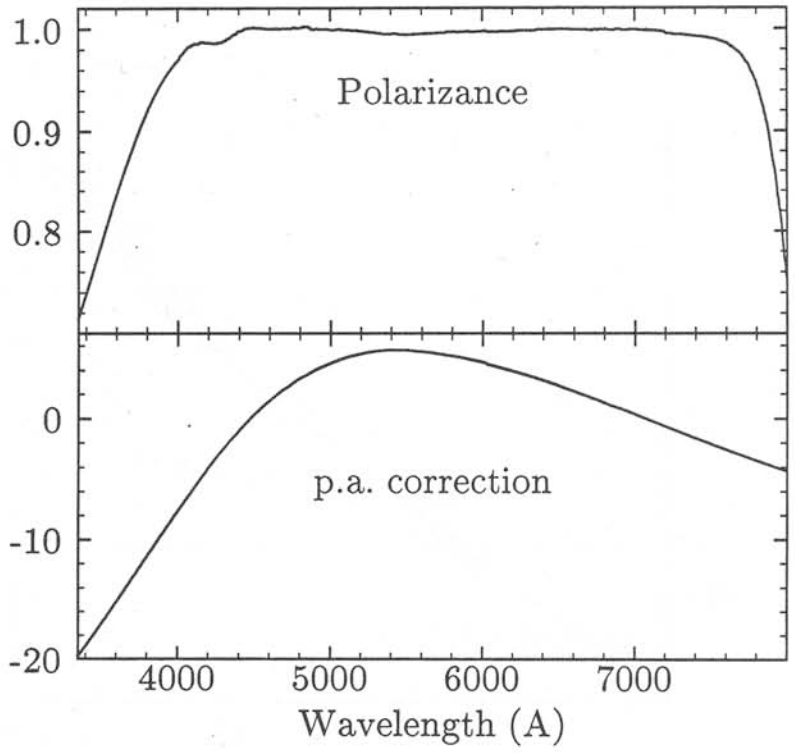

Figure 1. The measured polarizance and p.a. correction curves for the superachromatic halfwave plate now in use at the 3-m telescope. The fall-off in the polarizance to the red of 7600 Å is partly due to the failure of the calibration Polaroid to produce 100% polarized light at these wavelengths.

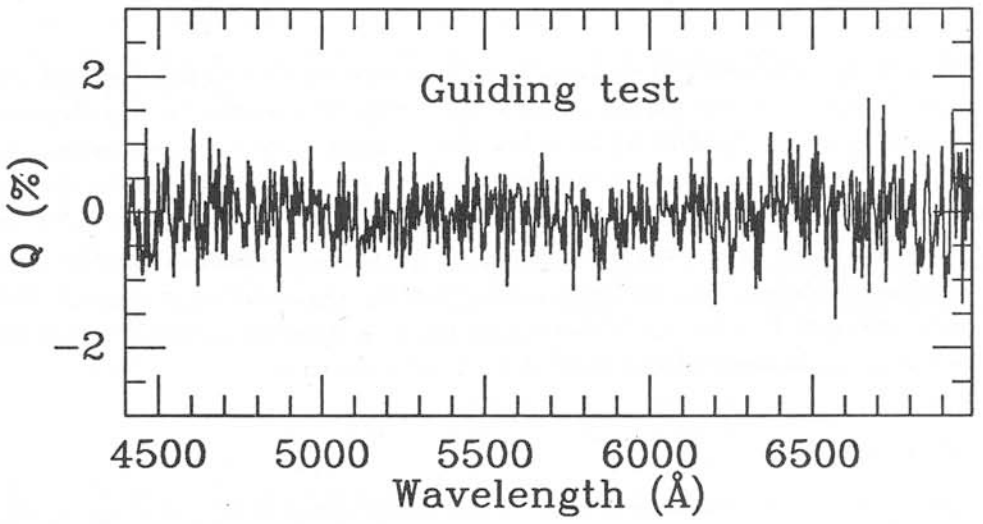

Figure 2. A purposely misguided exposure was used to test the ability of the instrument and the data reduction to correct for transparency, seeing, and guiding changes during a sequence of exposures. See text for detail.

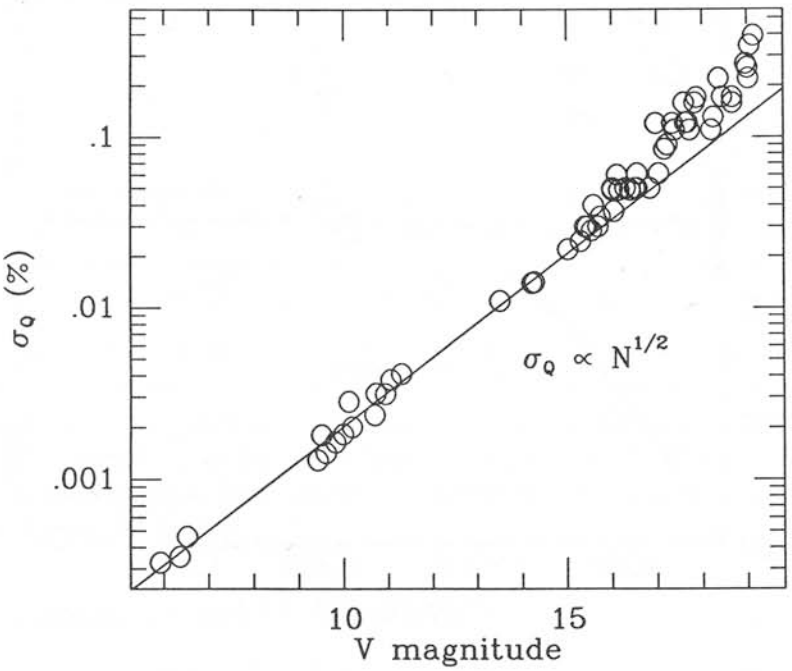

Figure 3. The weighted mean uncertainty as a function of V magnitude. The weighted mean is taken over all 800 pixels of the spectrum and is normalized to an exposure time of 10 minutes. Counting statistics from the object dominate down to V = 15.5 when noise in the sky begins to contribute.

All values of σ_Q have been normalized to an exposure time of 10 minutes and are the mean deviations of the entire, *weighted* spectrum. The scatter in this diagram is increased by using $f_\lambda(5500\ \text{Å})$ to define the V magnitude and then using this to represent the number of counts across the entire spectrum. The scatter is also increased by combining data from slightly different wavelength ranges, at different air masses, etc. The error analysis of the next section will describe how the σ_Q's are actually calculated. Here we simply note that the points follow a $\sigma_Q \sim N^{-1/2}$ line quite well until $V \sim 16$. At fainter magnitudes σ_Q is driven to higher values by the increasing importance of the night sky contribution to σ_Q.

3.4.5 Error analysis

For several reasons (not the least of which is our desire to use weighted means to get the optimum signal-to-noise in averaged Stokes parameters) we carefully follow the propagation of errors through our reduction formulae. Our assumptions are that we know the parameters (readout noise and gain) of the CCD very well and that the noise in the resulting spectra arise solely from readout noise and the statistical noise of counting statistics. Actual measurements of $\sigma(Q)$ when compared with our

calculated values of $\sigma(Q)$ indicate that these assumptions are indeed valid. If Fig. 3 were plotted with measured $\sigma(Q)$ along the y-axis rather than the calculated $\sigma(Q)$ it would be essentially identical.

For a given, single reduced spectrum (which we shall call "A", indicating either A_L, A_R, B_L, or B_R) we have

$$\sigma^2(A) = \sum_i \frac{S_i + r^2}{F_i^2} + \left(\frac{N_S}{N_B}\right) \sum_j \frac{B_j + r^2}{F_j^2}, \tag{5}$$

where r is the readout noise (all units are in electrons), S, B, and F represent intensities in the signal (object), background (sky), and flat field respectively, and N_S and N_B are the number of pixels summed to determine the signal and background levels respectively. Once the σ^2 of each of the four individual spectra are determined and the intensity correction, ω, applied we calculate

$$\sigma^2(Q) = \frac{4\omega^2}{(A + \omega B)^4} \left[A^2\sigma^2(B) + B^2\sigma^2(A)\right]. \tag{6}$$

If ω has been smoothed we further calculate

$$\sigma^2(< Q >) = \frac{1}{4}(\sigma_L^2 + \sigma_R^2), \tag{7}$$

where L represents the Q determined from A_L and ωB_L and R represents the Q determined from A_R and ωB_R.

It is traditional to report or display polarization data in the form of fractional (or percent) polarization and position angle, (p, θ), rather than in the Stokes parameters (Q, U). This is not, however, without serious drawbacks. The formula for p is positive definite

$$p = \sqrt{Q^2 + U^2} \tag{8}$$

which will always be positive even if the Q and U values are chosen from a symmetric probablity distribution centered around zero. Some authors (e.g. STOCKMAN and ANGEL [10]) advocate the use of the form

$$p = \pm\sqrt{|Q^2 + U^2 - \sigma^2(Q) - \sigma^2(U)|} \tag{9}$$

where the plus or minus sign is chosen dependent on the sign of $Q^2 + U^2 - \sigma^2(Q) - \sigma^2(U)$. The idea here is to "unbias" the expected value of p. This functional form, however, leads to a very peculiar probability distribution for p, which is shown in Fig. 4 for a relatively low signal-to-noise. Also shown in this figure is the probability distribution of the more standard, positive definite form for p. SERKOWSKI [11] gives this latter distribution as

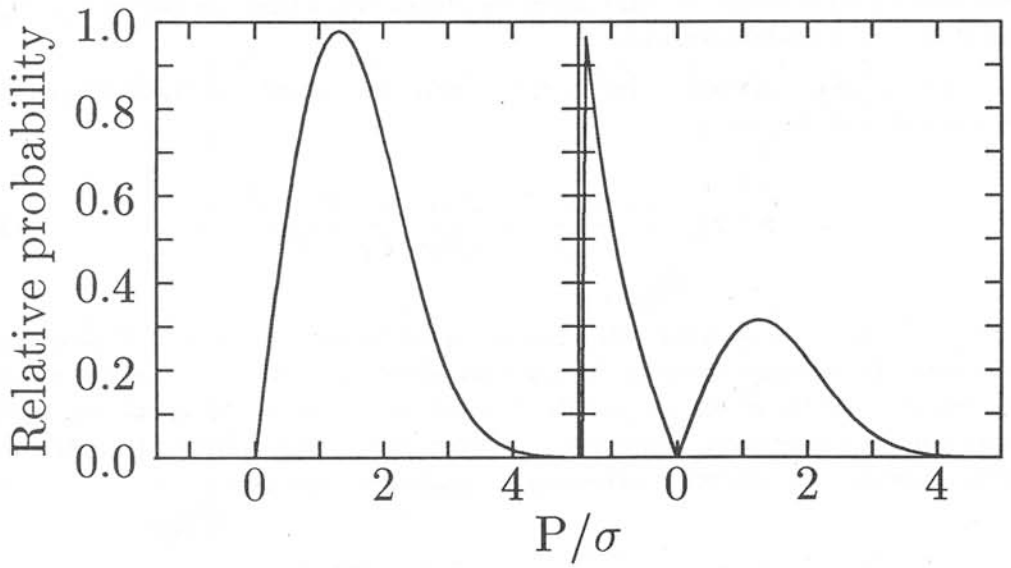

Figure 4. A comparison of the probability distributions of two forms commonly used to translate Q and U into polarization. In the left panel is the positive definite for and in the right panel the "unbiased" form preferred by some authors. A value of σ/Q=1 was used for these calculations.

$$f(p) = \frac{p}{\sigma^2}\, e^{-\frac{(p^2+p_0^2)}{2\sigma^2}}\, I_0(\frac{pp_0}{\sigma^2}), \tag{10}$$

where p_0 is the true value of polarization and σ is the uncertainty in Q and U.

The moral of this is to try to avoid if possible using p and θ. Hence all of our averaging, whether it is of multiple spectra or of all points within a single spectrum, is done in (Q, U) space. Then for publication the mean Q and U are often converted to (p, θ). Note, however, that in general the probability distribution of Q itself is not perfectly symmetric (CLARKE et al. [11]). In most cases we can safely ignore this asymmetry, and achieve a great savings in reduction time.

If we have a well-determined (Q, U) pair (i.e. $\sigma(Q)/Q \ll 1$) then the distribution of p becomes more symmetric and we may calculate $\sigma(p)$ and $\sigma(\theta)$ by

$$\sigma(p) = \frac{1}{p}\sqrt{Q^2\sigma^2(Q) + U^2\sigma^2(U)}$$

$$\sigma(\theta) = \frac{90^\circ}{\pi(Q^2+U^2)}\sqrt{Q^2\sigma^2(Q) + U^2\sigma^2(U)}. \tag{11}$$

3.4.6 Line polarizations

Often we are concerned with measuring the polarization of emission (or absorption) lines within a spectrum. For reasons mentioned in the preceding section it is not

advisable to attempt to measure these in the (p, θ) space but rather to stay in (Q, U) space. In this case we measure $Q(line)$ by forming the "Q Stokes flux," $F_\lambda Q$, and going through the normal procedure of defining and subtracting a continuum, defining the line limits and summing across the line profile. If $(F_\lambda Q)_c$ is the continuum level (taken for simplicity here as a constant across the line) this is mathematically

$$Q(line) = \frac{\sum[(F_\lambda Q)_i - (F_\lambda Q)c]}{\sum(F_{\lambda,i} - F_{\lambda,c})}. \tag{12}$$

Similarly, $U(line)$ is determined from $F_\lambda U$ and if desired p and θ of the line found. The errors in $Q(line)$ come from two sources, the pixel-to-pixel noise in $F_\lambda Q$, given by

$$\sigma_a^2[Q(line)] = \sum \frac{F_\lambda Q}{\sigma_i^2(Q)} \tag{13}$$

,

and the uncertainty in the determination of the continuum level, often quoted as a fraction, f, of the line flux

$$\sigma_b^2[Q(line)] \approx Q_L^2 f^2. \tag{14}$$

Hence

$$\sigma^2[Q(line)] = \sigma_a^2 + \sigma_b^2 \tag{15}$$

and the values of σ_p and σ_θ may be found as in the previous section.

3.4.7 Imaging Polarimetry

The previous discussion has centered on spectropolarimetry. Imaging polarimetry is done along similar lines with a few important exceptions. Some of the complications discussed below are equally applicable to spectropolarimetry and are noted.

One of the first steps in polarimetry reduction is the sky removal. The imaging polarimetry reduction procedure allows for a measurement of the sky level as free from personal bias as possible. An estimate of the sky level is input by the user, and an expected σ for this is used to identify all pixels within $\pm 2\sigma$ of the estimate. The mean of these pixels then replaces the initial sky estimate and the procedure is repeated for this value. After a small number of iterations the sky value has converged and this value is then assumed to be the true sky level. In images in which there is only a very small number of pixels close to the sky level the user may opt to define a box in which the sky is calculated. No iterations are performed in this case, as the same box is used to calculate the sky in all images.

This method will tend to estimate a sky level higher than the true value because some pixels near the detected edge of the target object will be included in the $\pm 2\sigma$ cutoff. This will also occur if the object is so extended that *no* pixels contain only sky. This latter situation can also occur in the spectropolarimetry reduction. However, because each of the four individual images used to calculate a

Stokes parameter are treated identically there is no change in the polarization p.a. and only a change in the "dilution" of the polarization level itself. To make this clearer consider the case of an object like the Seyfert 2 galaxy NGC 1068, which is so large that it overfills our imaging and spectropolarimetry fields. By including some of the galaxy's starlight in the sky subtraction we are effectively also removing some starlight from the nucleus. However, in as much as the starlight is unpolarized we are only removing part of a "diluting" source, and the net result will be a small increase in the measured polarization.

In spectropolarimetry the telescope guiding is usually done directly off of the slit jaws, and hence the spectra always fall on the same pixels. In imaging polarimetry, however, the slit jaws are opened much wider (to $40''$) and the amount of slit left on which we can guide is much more restricted. In some cases we cannot guide at all, having to rely on accurate drive rates and short exposure times to minimize image drift. To compensate for changing image position between exposures we use a cross-correlation to determine offsets between pairs of images, then shift the images before calculating the Stokes parameter via eq. (2).

This latter problem of having to shift images to overlay them brings up the difficult problem of possible undersampling of the data and the consequent uncertainty in how to interpolate them in the shifting procedure. In fact ideally one would like to match point-spread functions among all of the frames! The overhead in computing time for such a procedure becomes very large and we have chosen to forego this refinement and take care in interpreting data containing steep gradients in flux — as these are the most difficult to interpolate properly. The reduction system also provides an option for smoothing the data by an arbitrary amount before shifting, thus increasing the effective sampling but decreasing the angular resolution of the data. We note that the undersampling is not nearly such a grave problem in spectropolarimetry. To extract a 1-D spectrum from a 2-D image we typically sum over 7 to 14 pixels, and thus use an effective over-sampling of the data. In the dispersion direction the separation between the L and R spectra depends only on the rotation of the beamsplitter in its holder, something which is very stable. Potentially, however, the undersampling in the dispersion direction could be a concern in some spectropolarimeter designs.

A final point to be mentioned is the method by which ω, the balance factor defined in eq. (3), is calculated. One possible technique is to simply calculate ω pixel by pixel and then to take the mean of these values. But since ω is a ratio this technique leads to a bias of ω to values higher than the true value. Our technique is to sum all of the photons in the four *sky-subtracted* images from which the Stokes parameter is calculated. Calling these sums A_L, A_R, B_L, and B_R we then calculate ω using eq. (3). This provides a more accurate value for the balance factor.

4. Concluding Remarks

The CCD spectrograph and spectropolarimeter described above works extremely well. It represents an increased efficiency over the older Pockels cell ITS device by nearly a factor of 20. Much of the gain comes from the much higher quantum efficiency of the CCD detector, but additional gains are realized because of the

higher polarizance and more accurate sky subtraction. Also there is the added bonus of the imaging polarimetry mode; an example of the use of this is given in a paper by Goodrich [13].

At present ultraviolet observations must be made with the calcite crystal with its more restrictive field of view, because the polarizing cubes do not transmit in the UV. However, we are currently developing a new set of cubes using sapphire as the substrate, which should provide greatly improved UV performance.

Our use of the device is concentrated on studies of active galaxies and QSOs. The high efficiency means that we can routinely observe objects as faint as magnitude 18, though of course for the faintest objects the data are more limited in spectral resolution or signal-to-noise; a similar device is planned for the Keck 10-m telescope.

Acknowledgements

We wish to thank Vinod Vats of Karl Lambrecht Corporation for his efforts in producing the highly successful beam-splitting polarizing cubes and Tom Baur of Meadowlark Optics for his care and efforts in manufacturing the excellent half-wave retarder. This research was supported in part by NSF grant AST 84-06843.

References

1. J.S. Miller, L.B. Robinson, G.D. Schmidt: *Pub. A.S.P.*, **92**, 702 (1980).

2. L.B. Robinson: 1987 Santa Cruz Summer Workshop.

3. L.B. Robinson, R.J. Stover, J. Osborne, J.S. Miller, S.S. Vogt, S.L. Allen: *Optical Engineering*, **26**, 795 (Aug. 1987).

4. C.D. Mackay: *S.P.I.E.* **331,** 146 (1982).

5. J.T. McGraw, H.S. Stockman, J.R.P. Angel, H. Epps: *S.P.I.E.* **331,** 137 (1982).

6. J.R. Janesick: private communication.

7. J.R. Janesick, T. Elliot, S. Collins, M.M. Blouke, J. Freeman: *Optical Engineering* **26,** 703 (Aug. 1987).

8. J.R. Janesick, M.M. Blouke: 1987 Santa Cruz Summer Workshop.

9. T. Lauer, R. Stover, and D. Terndrup: *Lick Observatory Technical Report No.33* (1984).

10. H.S. Stockman and J.R.P. Angel: *Ap.J. (Letters)*, **220**, L67 (1978).

11. K. Serkowski: *Adv. in Astron. Astrophys.*, **1**, 289, ed. Z. Kopal (N.Y. and London: Academic Press) (1962).

12. D. Clarke, B.G. Stewart, H.E. Schwarz, and A. Brook: *Astron. Astrophys.*, **126**, 260 (1983).

13. R.W. Goodrich: *Ap.J.* **311**, 882 (1986).